*Journal of Geophysical Research*

Supporting Information for

# $SO_2$ oxidation kinetics leave a consistent isotopic imprint on volcanic ice core sulfate

Elsa Gautier[1], Joel Savarino[1], Joseph Erbland[1] and James Farquhar[2]

[1]Université Grenoble Alpes, CNRS, IRD, Grenoble INP, IGE, 54 Rue Moliere, F-38000 Grenoble, France

[2]University of Maryland, Department of Geology, 8000 Regents drive, College Park, MD 20742, USA

## Contents of this file



## Introduction

The supporting information includes:

- A detailed description of the method used to obtain our results: Samples processing, isotopic analysis, background correction and uncertainties (Text S1, Tables S1, S2, S3)
- A calculation of the weighted isotopic budget for 10 events (Table S4)
- An explanation of the modeling of sulfate isotopic composition: principle, results and interpretation (text S2, Table S5, Figure S1)
- Additional figures (Figure S2, S3)
- A dataset of all data used in the study (Dataset S1), also uploaded separately

## Text S1. Details of method and materials

## 1. Sample processing

Multiple cores were necessary to guarantee enough sulfate for a time-resolved isotopic analysis of each volcanic events identified in the ice. For this reason, five cores were drilled 1m from each other, during the 2010/2011 summer campaign in Dome C (Antarctica, 75°06'S, 123°21'E, elevation 3220 m, mean annual temperature -54.5°C). After decontamination by scraping the outer surface of the core with a scalpel, a lamella is cut lengthwise, with a band saw, sampled with a 2cm-resolution. They were entirely processed for sulfate concentration profiles directly in Concordia station. Analyses were performed on Metrohm IC (Professional 850), in a fast IC configuration (2 minutes run) to quantify sulfate. The mean annual snow accumulation rate at Dome C is 10 cm of snow/year (25 kg $m^{-2}$ $a^{-1}$); the estimated time-period covered by the cores is 2600 years.

Once obtained, the five sulfate profiles have been processed with an algorithm for peak detection. The algorithm allowed us to identify a total of 63 sulfate peaks above the sulfate background, attributed to potential volcanic events [for details see (Gautier, 2015; Gautier et al., 2016)]. Once volcanic peaks were identified, the ice sections containing the volcanic events were brought back at IGE (Institut des Géosciences de l'Environnement, former Laboratoire de Glaciologie et de Géophysique de l'Environnement) for further processing. After decontamination of the ice sections, the ice containing specific volcanic events was isolated from the rest of the core (sawed in a cold room) and subsampled at least in 5 portions, composed of two backgrounds (before and after the peak) and at least 3 parts for the volcanic peak. The choice of sub-sampling meets two needs: Firstly, the background samples allow for the correction of the volcanic peak isotopic composition from the background contribution. Secondly, the peak subdivision allows following the time-evolution of the volcanic isotopic signal.

Each event has been subdivided the same way on the 5 replicate cores. The five logs of the same deposition stage were then gathered together and melted. In the resulting samples, of roughly two liters, sulfate was extracted with an ion chromatograph (Metrohm professional 850 IC) used in a semi preparative configuration. The sample is first loaded in a guard column (Dionex AG15 4x50mm) with a flow rate of 4 mL/min, for pre-concentration of the anions. When the sample is entirely pre-concentrated, anions are separated in a second column (Metrosep A supp 16, 250/4) using a NaOH eluent in gradient mode (NaOH solution 10-50 mM). After the column separation, a $H^+$ cation-exchange column neutralizes the eluent. A conductivity detector follows the elution of the anions and when the sulfate elutes, the flow is diverted to collect the sulfate sample. Tests have shown that the recovery of initial sulfate approaches 100 %. In a single step, the sulfate sample is thus purified, converted to pure $H_2SO_4$ and concentrated in a volume lower than 10 ml quantitatively. $H_2SO_4$ samples, prepared in IGE Grenoble, were then shipped to the University of Maryland, where we performed the isotopic analysis.

## 2. Isotopic analysis

$H_2SO_4$ samples, concentrated in a total liquid volume bellow 10ml, were reacted with a heated Thode solution, consisting of a (3.3:2:1) mixture of concentrated hydrochloric, hydroiodic and hypophosphorous acids (Thode et al., 1961) flushed by a $N_2$ flux, during 4 hours. Sulfate, reduced to hydrogen sulfide ($H_2S$), was carried by the $N_2$ stream through a Milli-Q water trap, and finally precipitated in a 0.03M $AgNO_3$ solution to form silver sulfide ($Ag_2S$). This precipitate would stand in the capture solution and be aged in the dark for a week to dissolve impurities. After several rinsing steps in 1M $NH_4OH$ and Milli-Q water, $Ag_2S$ was dried and loaded in a

handmade aluminum capsule. Introduced in heated nickel bombs previously pumped, the sample was reacted overnight with fluorine ($F_2$ gas), introduced in excess in the bombs. The resulting $SF_6$ gas was separated from $F_2$ and HF through cryogenic distillation steps. After a last purification step, through gas chromatograph, the $SF_6$ sample was collected in a glass manifold and brought to the dual inlet mass spectrometer ThermoFinnigan Mat 253. Taking into account the small sulfur amount of the samples (between 0.8 and 2 µmol, for most of them), $SF_6$ samples and reference gas were transferred and cryofocused in very small volumes, isolated from the bellows, in order to maximize the signal to noise ratio and to stay in the viscous flow regime (Au Yang et al., 2016). 3 to 4 runs of 10 analyses were conducted for each sample, and 127, 128, 129 and 131 mass ratios were measured (respectively $^{32}SF_5^+$, $^{33}SF_5^+$, $^{34}SF_5^+$ et $^{36}SF_5^+$).

**3. Background correction**

The isotopic composition of non-volcanic ice core sulfate is determined by contributions from biogenic sulfate ($nssSO_4^{2-}$ coming from dimethyl sulfide oxidation), minor sea salt aerosols (less than 10% to the sulfate background) and near negligible background stratospheric sulfate from the Junge layer (Junge et al., 1961). Biogenic sulfate has variable $\delta^{34}S$ in the range 14 to 22 ‰ (Oduro et al., 2011; Patris et al., 2000); the $\delta^{34}S$ of sea salt sulfate aerosols is 21 ‰ (Rees et al., 1978) and background stratospheric sulfate has a constant $\delta^{34}S$ of 2.6 ± 0.3 ‰ in both hemispheres (Castleman et al., 1974). Both $\Delta^x S$ and $\delta^x S$ are corrected from background-sulfate contributions in order to characterize the post-stratospheric volcanic plume.

We estimate background sulfate composition by sampling time before and after each volcanic peak, and make the implicit assumption that it will be representative of the background during the sulfate peak deposition. We will see in the following that we have good reasons to consider that mass dependent and mass independent fractionation of sulfur are happening simultaneously, in the stratosphere, and that subsequent processes slightly impact the isotopic signal. We characterize the concentration and isotopic composition of the background for each volcanic event to determine the volcanic signal. For background calculation, we took the mean value of two background samples, taken before and after the eruption peak. When background values are missing for a given volcanic event (sample lost or too small to have reliable isotopic measurements), isotopic data for this event are corrected considering the average of the 18 background values we measured (see below). All background concentrations and isotopic values are gathered in Table S1 and display no isotopic anomaly.

On average, the sulfate mass fraction is 89 $ng.g^{-1}$ (with a 10 $ng.g^{-1}$ standard deviation), and background isotopic composition is 15 ‰, 0.05 ‰ and 0.3 ‰, for $\delta^{34}S$, $\Delta^{33}S$ and $\Delta^{36}S$ respectively. Although quite steady, variability between the different background values is noticeable ($2\sigma$ = 2.7, 0.1 and 1.3 ‰ for $\delta^{34}S$, $\Delta^{33}S$ and $\Delta^{36}S$ respectively), hence the need to sample background for each volcanic event.

The sample is composed of a background fraction ($f_{bg} = {[SO_4^{2-}]_{bg}}/{[SO_4^{2-}]_{total}}$) and a volcanic fraction ($f_v = 1 - {[SO_4^{2-}]_{bg}}/{[SO_4^{2-}]_{total}}$). We make the trace abundance approximation, and background corrections are achieved through the following mass balance equation:

$$\delta_v = {(\delta_{meas} - f_{bg} . \delta_{bg})}/{f_v}$$

Where $\delta_v$ is the isotopic value of the volcanic plume (after passing the stratosphere), $\delta_{meas}$ is the measured isotopic value of our sample, $\delta_{bg}$ is the isotopic composition of the background.

**4. Uncertainty**

The total uncertainty of the volcanic isotope data results from three distinct, cumulative errors: the internal error related to the mass-spectrometer precision, the external error that takes into account the entire analytical pathway, and the error propagation emerging from background corrections.

*4.1 Internal error*

The internal error associated with the MAT 253 of University of Maryland is typically: better than 0.012‰, 0.006‰ and 0.05 ‰ for $\delta^{33}S$, $\delta^{34}S$ and $\delta^{36}S$ respectively, but it can rise depending on the sample size.

*4.2 External error*

To estimate the method reproducibility, from the concentration to the isotopic analysis, external standards went the same way as volcanic samples: A $Na_2SO_4$ solution was run through the IC to make $H_2SO_4$ standards of different concentrations. These sulfate standards were then reduced, fluorinate, purified and analyzed in the usual conditions. We thus obtained the external error. Values are quite high, which is not surprising given the number of steps in the analysis.

*4.3 Error propagation*

When correcting isotopic values from the background contribution (Table S1), error propagation has to be taken into account. For error propagation calculation, un-corrected sample errors were assumed to be under the following values: (1σ= 0.6, 0.02 and 0.1‰) for $\delta^{34}S$, $\Delta^{33}S$, $\Delta^{36}S$ respectively.

The determination of the isotopic composition of the background biogenic sulfate is also a source of error. When comparing all background measured from the different events, it appears that variability among them is (2.1, 0.08 and 0.4‰) for $\delta^{34}S$, $\Delta^{33}S$, $\Delta^{36}S$ respectively. This variability is not surprising given that the background is a natural contribution that can vary in time.

We used a Monte-Carlo routine to build a synthetic dataset of 10 thousand dual isotopic compositions sample – blank, leading to a dataset of 10000 volcanic isotopic compositions, on which uncertainties were estimated. Considering uncertainties previously described for samples and background, we estimated uncertainties arising from background correction for different volcanic fractions in the total sample. All samples with a volcanic contribution above 20% were corrected from their background contribution ($f_{bg}$). However, given uncertainties arising from such corrections (Table S3), and to avoid a significant bias in trends, only samples with a volcanic fraction of at least 65% were plotted when considering $\Delta^{36}S$ and $\Delta^{33}S$ trends.

*4.4 Error on slopes*

The 1-σ uncertainty on slopes are calculated following recommendation in (Taylor, 1997), p188 where data are fitted by a straight line using the least-squares method. In this situation, uncertainty of the slope is defined as:

$$\sigma_{B=\sigma_y}\sqrt{\frac{N}{(N\sum x^2-(\sum x)^2)}}$$

Where B is the slope deduced from the least-square, $\sigma_y$ the uncertainty of the measurements that includes both the uncertainty of $\Delta^{33}S$ and $\Delta^{36}S$ and N, the number of analysis.

**Text S2. Modeling sulfate isotopic composition**

*1. Principle*

The model used to simulate the isotopic composition of stratospheric sulfate is encoded in the python language. In the initial conditions, the $SO_2$ is not fractionated ($\delta^{33}S = \delta^{34}S = \delta^{36}S = 0$), and is a limited reservoir. At each iteration, a given amount of $SO_2$ is oxidized through 3 different pathways, with different fractionation factors. We show the modeled isotopic composition in the resulting sulfate.

Fractionation factors for photochemical processes are taken from (Whitehill et al., 2015) (Table 3, *T=250K*, and Table 4, $PO_2$*=5.07 kPa* for photoexcitation and photolysis respectively) and (Whitehill & Ono, 2012) (calculated from elemental sulfur enrichment in Table 1) and (Endo et al., 2016) (self shielding fractionation, text part 3.5). Fractionation factor $\alpha^{34}$ of the MDF OH oxidation pathway is obtained through the temperature dependent relation from (Harris et al., 2012) (1.0089-0.00004*T/°C), using a temperature of -40°c, representative of stratospheric conditions at 30km height. $\alpha^{36}$ and $\alpha^{33}$ are deduced through mass dependent relationships ($\alpha^{33} = (\alpha^{34})^{0.515}$; $\alpha^{36} = (\alpha^{34})^{1.9}$).

*2 Simulation of S-MIF pattern, results and interpretation*

The model enables to reproduce broadly the isotopic signature observed in the deposited sulfate (Fig. S1A) and gives the isotopic trends obtained for given fractionation factors and mechanism-specific proportions in the oxidation step (Fig. S1B).

Using (Whitehill et al., 2015) fractionation factors for both photolysis and photo-excitation, and (Harris et al., 2012) fractionation factors for OH oxidation, it emerges that to reproduce the set of trends we observe in volcanic sulfate:

- the proportion of photolysis must be 6 times higher than the proportion of photo-excitation (this mixing controls the $\Delta^{36}S$ / $\Delta^{33}S$ slope)
- the proportion of mass-dependent processes (OH oxidation) must be 10% while the proportion of mass-independent processes would be 90% (this mixing controls the $\Delta^{33}S$ / $\delta^{34}S$ slope).

This minor contribution of OH oxidation contradicts our current knowledge of oxidation pathway in the stratosphere (Bekki, 1995; Seinfeld & Pandis, 1998). Several explanations can be considered. First, the fractionation factors used in the simulation do not represent the processes taking place in the stratosphere, second, the fractionation factors are affected and diluted by mass dependent processes in the experimental cell of (Whitehill et al., 2015); likely

due to the presence of $O_2$, and $H_2O$ leading to the formation of OH. This would explain why we need such a high proportion of mass independent processes to reproduce the volcanic slopes. Third, stratospheric chemistry as currently understood is partly wrong, and the role of OH-oxidation has been largely overestimated. Stratospheric ozone can be severely depleted after an eruption (Cadoux et al., 2015; von Glasow, 2010), due to volcanic halogen emissions (chlorine and bromine). OH would in that case be largely depleted during a few weeks after the eruption (Bekki, 1995; Hattori et al., 2013; von Glasow, 2010), and could, under these conditions, play a less important role in sulfur dioxide oxidation. OH titration by an excess of $SO_2$ would also lead to a self-limitation of this pathway, and decrease its role in the oxidation process. Even under such conditions, it would be surprising to have only 10% of OH oxidation, but the possibility is not nil.

Using the (Endo et al., 2016) fractionation factors for photolysis, (Whitehill & Ono, 2012) fractionation factors for photo-excitation, and (Harris et al., 2012) factors for OH oxidation leads to more expected results: 80% of OH oxidation, and 20% of photolysis plus photo-excitation (in a 7:1 ratio), and a value of $\Delta^{33}S$ that could possibly be found in volcanic sulfate collected in the ice (note that all our $\Delta^{33}S$ values are diluted due to the time resolution of the sampling. Each sample covers two years on average) (Fig. S1*B*).

(a)

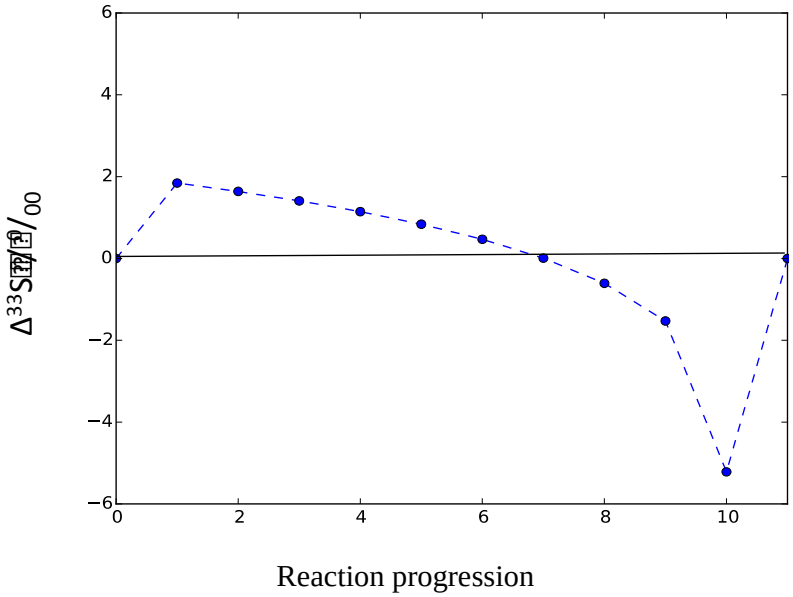

(b)

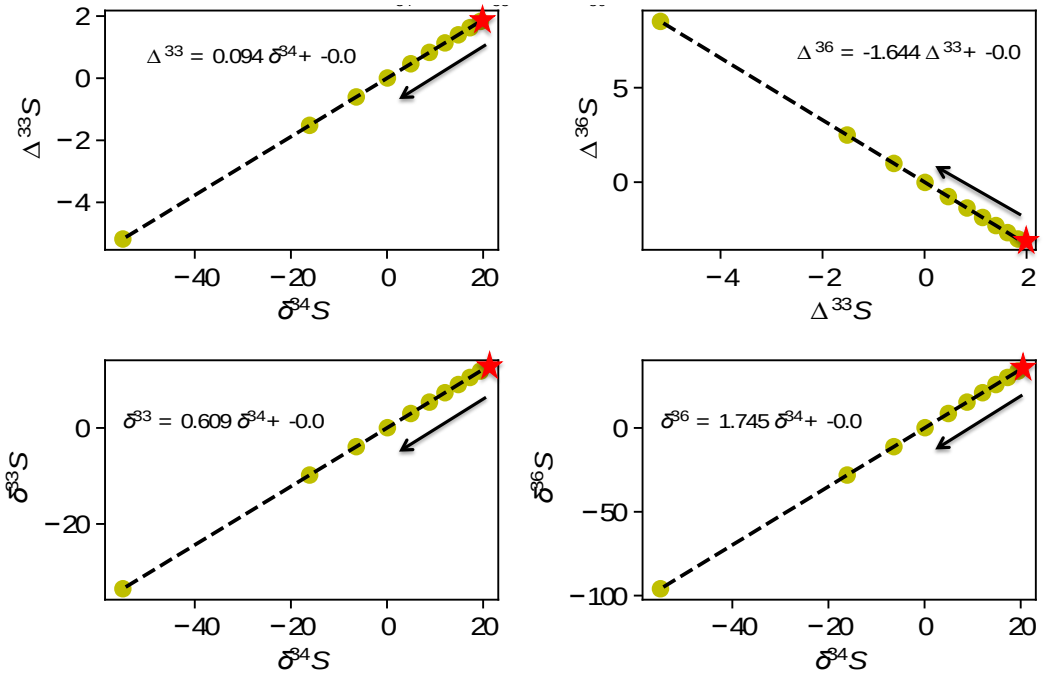


photolysis : 20.0% photoex : 3.0% : $\varepsilon_{34}$ = 1.054/1.0185 ; $\varepsilon_{33}$ = 1.03481 / 1.0248 ; $\varepsilon_{36}$ = 1.0859/1.0454
OH-oxidation : $\varepsilon_{34}$ = 1.0105 ; $\varepsilon_{33}$ = 1.0054 ; $\varepsilon_{36}$ = 1.02

**Figure S1.** A - Pattern obtained by simulating $\Delta^{33}S$ vs. time (time is virtually represented by iteration steps in the model and has no physical meaning. Progression 0 corresponds to the beginning of the $SO_2$ reservoir oxidation; progression 11 marks the complete exhaustion of the $SO_2$ reservoir). The pattern is clearly asymmetric with a long and small positive phase (as much as the observation), and a short and sharp negative phase which may explain why the negative phase is more difficult to detect in the deposited ice record (e.g. it gets deposited elsewhere) (Table S4). The isotopic budget is zero.
B – Set of trends illustrating the evoluting composition of sulfate formed during the process of oxidation of volcanic $SO_2$. The red star corresponds to the composition of the first formed sulfate. Subsequent formed sulfates follow the direction of the black arrow. This set is obtained using (Harris et al., 2012) OH fractionation factors, (Endo et al., 2016.; Whitehill and Ono, 2012) for photolysis and photoexcitation respectively. The proportions of each mechanism used as input for this result are : 20% of photolysis, 3% photoexcitation, 77% OH-oxidation. Isotopic values are given in per mill. The slopes obtained with such inputs are similar to the results obtained for natural volcanogenic sulfate.

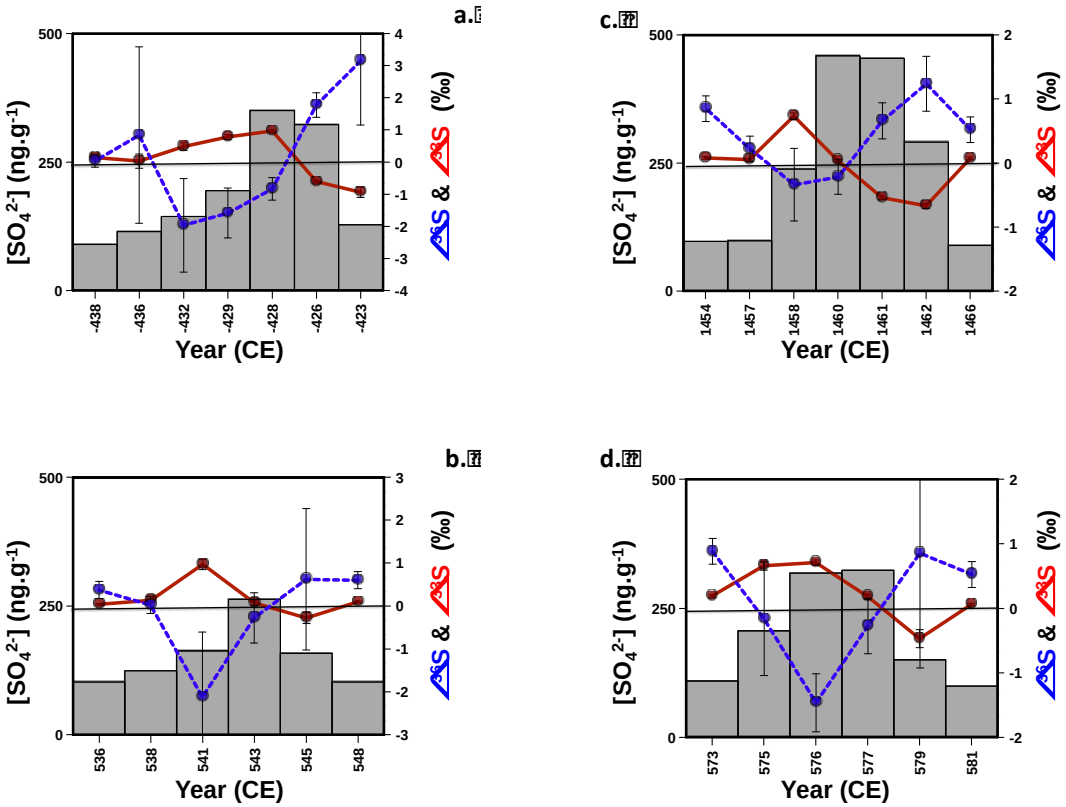


254

255 (a)
256
257

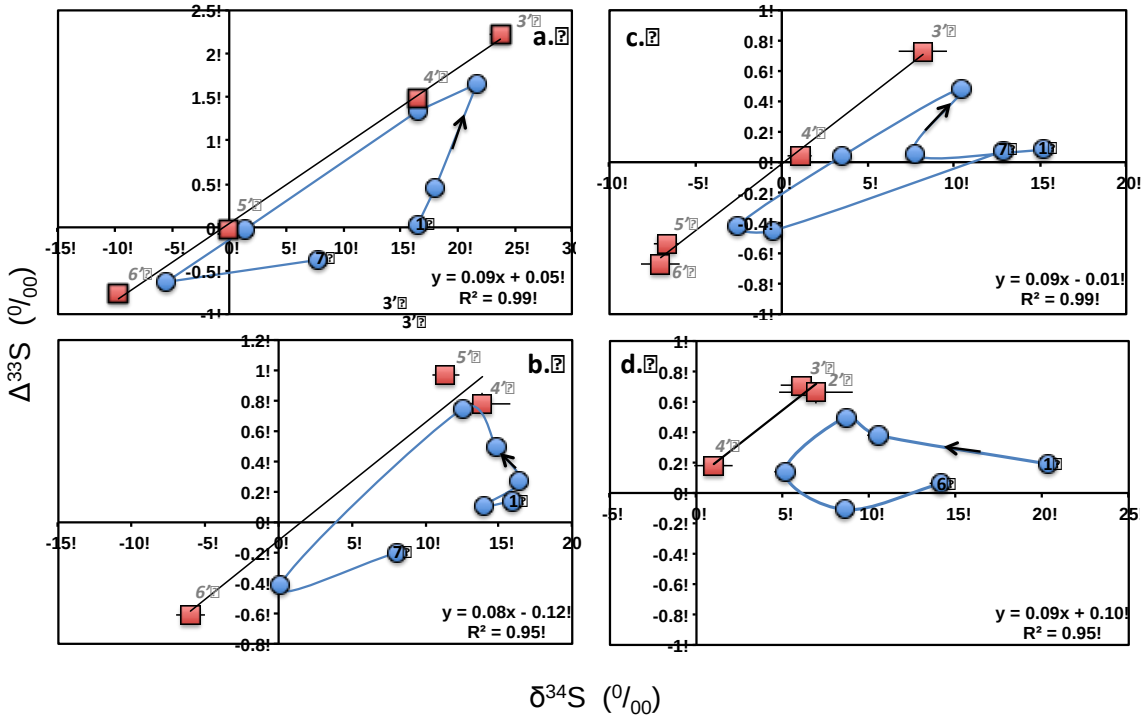


**(b)**

**Figure S2.**

(a) $\Delta^{36}S$ and $\Delta^{33}S$, plotted vs. time four 4 different volcanic events: a: Event 49: 540 BCE - b: Event 30: 540 - c: Event 13-Kuwae: 1459 – d: Event 31: 576. Grey boxes represent the concentration of sulfate, expressed as mass fractions (in $ng.g^{-1}$) in the samples. Red dots (plain line) are $\Delta^{33}S$ values, blue dots (dashed line) are $\Delta^{36}S$, both are background corrected when volcanic sulfate is above 40% in the sample.

(b) Cross plot of $\Delta^{33}S$ vs. $\delta^{34}S$ for 4 different volcanic events: a: Event 16-Samalas: 1259 - b: Event 49: 426 BCE - c: Event 13-Kuwae:1459 – d: Event 30: 576 . Blue dots are data uncorrected from background. Red dots are points mostly volcanic (more than 40%), after correction from the background contribution. Invisible uncertainties are included in the size of the point.

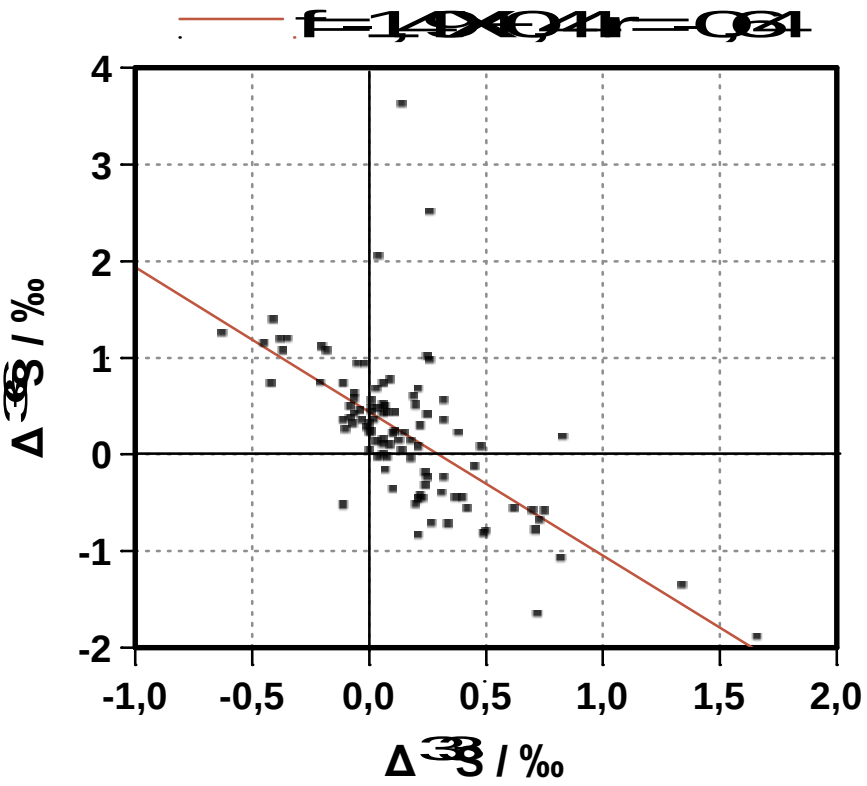


**Figure S3**. Cross plot of **$\Delta^{36}S$ vs. $\Delta^{33}S$.** Plotted data points are not background corrected values; the slope is not affected by background mixing. Note that the background contribution only arises from mass dependent processes and dilutes $\Delta^{36}S$ and $\Delta^{33}S$ in the same proportion. As a result, corrected or uncorrected data do not fundamentally change the $\Delta^{36}S$ / $\Delta^{33}S$ slope, only the absolute values are affected.

| Volc. event | $\delta^{33}S$ | $\delta^{34}S$ | $\delta^{36}S$ | $\Delta^{33}S$ | $\Delta^{36}S$ | $[SO_4^{2-}]$ |
|---|---|---|---|---|---|---|
| Ev 06 BGD | 7.885 | 15.238 | 29.805 | 0.066 | 0.654 | 74 |
| Ev 10 BGD | 6.422 | 12.68 | 24.533 | -0.088 | 0.303 | 70 |
| Ev 13 BGD | 7.279 | 14.041 | 27.534 | 0.072 | 0.687 | 94 |
| Ev 15 BGD | 8.495 | 16.567 | 32.388 | -0.003 | 0.677 | 81 |
| Ev 16 BGD | 8.342 | 16.087 | 31.148 | 0.09 | 0.362 | 81 |
| Ev 17 BGD | 7.831 | 15.148 | 26.809 | 0.058 | -2.169 | 76 |
| Ev 22 BGD | 7.559 | 14.528 | 28.757 | 0.103 | 0.974 | 91 |
| Ev 30 BGD | 7.397 | 14.262 | 27.838 | 0.077 | 0.566 | 101 |
| Ev 31 BGD | 7.842 | 15.151 | 29.478 | 0.068 | 0.495 | 103 |
| Ev 35 BGD | 7.625 | 14.756 | 28.788 | 0.052 | 0.566 | 87 |
| Ev 37 BGD | 7.062 | 13.627 | 26.798 | 0.067 | 0.748 | 97 |
| Ev 38 BGD | 7.148 | 13.911 | 27.315 | 0.008 | 0.72 | 108 |
| Ev 44 BGD | 6.379 | 12.312 | 23.705 | 0.057 | 0.182 | 92 |

| | | | | | | |
|---|---|---|---|---|---|---|
| Ev 46 BGD | 8.121 | 15.696 | 30.492 | 0.068 | 0.459 | 94 |
| Ev 48 BGD | 7.859 | 15.256 | 29.633 | 0.031 | 0.447 | 84 |
| Ev 49 BGD | 8.318 | 15.934 | 30.528 | 0.143 | 0.036 | 97 |
| Ev 50 BGD | 8.692 | 16.813 | 32.362 | 0.068 | 0.176 | 90 |
| Ev 51 BGD | 8.953 | 17.366 | 33.537 | 0.047 | 0.283 | 91 |
| **Average** | **7.73** | **14.97** | **28.97** | **0.05** | **0.34** | **89** |
| **Stand. dev.** | **0.71** | **1.36** | **2.63** | **0.05** | **0.67** | **10** |
| 2σ | 1.42 | 2.72 | 5.27 | 0.10 | 1.34 | 20 |

**Table S1**. Background composition of volcanic events, and background average value, used to correct volcanic data when background value was not known. Isotopic data are given in per mil. Sulfate amount in the sample is given in $ng.g^{-1}$.

| $n(SO_4^{2-})$ (µmol) | $\delta^{33}S$ (‰) | $\delta^{34}S$ (‰) | $\delta^{36}S$ (‰) | $\Delta^{33}S$ (‰) | $\Delta^{36}S$ (‰) |
|---|---|---|---|---|---|
| 3 | -1.58 | -3.00 | -5.64 | -0.04 | -0.12 |
| 6 | -1.73 | -3.33 | -6.09 | -0.02 | 0.05 |
| 4 | -1.24 | -2.36 | -4.47 | -0.03 | -0.16 |
| 4 | -1.98 | -3.89 | -7.38 | 0.01 | -0.18 |
| **std. dev. σ (‰)** | 0.31 | 0.64 | 1.20 | 0.02 | 0.11 |
| **2 σ** | 0.62 | 1.27 | 2.41 | 0.05 | 0.21 |

**Table S2**. Isotope measurements of internal standards that underwent the entire process, from the IC concentration step to $SF_6$. These measurements allow getting $\delta^{33}S$, $\delta^{34}S$ or $\delta^{36}S$, $\Delta^{33}S$ and $\Delta^{36}S$ standard deviations, i.e the external error specific to our analysis chain that must be taken into account for our samples isotopic measurements.

| Volcanic fraction | $1\sigma$ - $\delta^{34}S$ | $1\sigma$ - $\Delta^{33}S$ | $1\sigma$ - $\Delta^{36}S$ |
|---|---|---|---|
| **0.9** | 0.68 | 0.02 | 0.24 |
| **0.8** | 0.82 | 0.03 | 0.30 |
| **0.7** | 1.03 | 0.04 | 0.41 |
| **0.6** | 1.34 | 0.05 | 0.55 |
| **0.5** | 1.80 | 0.06 | 0.78 |
| **0.4** | 2.53 | 0.09 | 1.13 |
| **0.3** | 3.75 | 0.13 | 1.69 |
| **0.2** | 6.21 | 0.23 | 2.87 |
| **0.1** | 13.70 | 0.52 | 6.49 |

**Table S3.** Uncertainties arising in isotopic values with decreasing volcanic contribution in total sulfate, obtained through Monte Carlo error propagation method.

| Event | Positive weighted isotopic budget | Total weighted isotopic budget | % of loss of the negative part of the signal | % of loss of the positive part of the signal |
|---|---|---|---|---|
| 6.1 | 0.40 | -1.45 | | 78 |
| 6.2 | 0.47 | 0.37 | 77 | |
| 10 | 4.89 | 4.35 | 89 | |
| 16.4 | 9.12 | 4.96 | 54 | |
| 17 | 5.02 | -0.48 | | 9 |
| 22 | 3.06 | 3.06 | 100 | |
| 30 | 2.79 | 1.71 | 61 | |
| 31 | 3.41 | 3.25 | 95 | |
| 46.1 | 4.30 | 4.07 | 95 | |
| 49 | 5.28 | 0.28 | 5 | |

**Table S4**. Isotopic budget on volcanic events completely analyzed (no missing sample). Very frequently a large part of the negative signal is missing in the global budget.

| *Fractionation factor* | *OH - oxid* | *Photolysis whitehill15 / Endo16* | *Photoexcitation Whitehill15 / Whitehill12* |
|---|---|---|---|
| $\alpha^{34}$ | 1.0105 | 1.08924 / 1.054 | 1.00733 / 1.0184 |
| $\alpha^{33}$ | 1.0054 | 1.05085 / 1.03481 | 1.02529 / 1.0248 |
| $\alpha^{36}$ | 1.02 | 1.15093 / 1.0859 | 1.06439 / 1.0454 |

**Table S5**. Fractionation factors used in the study

| Sample | Top depth (m) | estimated age | $SO_4^{2-}$ (ppb) | Volc. fraction $f_V$ | $\delta^{33}S$ | $\delta^{34}S$ | $\delta^{36}S$ | $\Delta^{33}S$ | $\Delta^{36}S$ | $\sigma(\delta^{34}S)$ | $\sigma(\Delta^{33}S)$ | $\sigma(\Delta^{36}S)$ |
|---|---|---|---|---|---|---|---|---|---|---|---|---|
| Ev 3.2-5 | 8.86 | 1886.2 | 179.6 | 0.6 | 0.81 | 1.35 | 3.54 | 0.12 | 0.96 | 1.53 | 0.05 | 0.62 |
| Ev 3.2-6 | 8.98 | 1884.3 | 88.45 | 0.19 | 7.91 | 15.02 | 29.6 | 0.2 | 0.87 | 0.6 | 0.02 | 0.2 |
| Ev 4.0-4 | 10.46 | 1861.4 | 79.43 | 0.25 | 13.01 | 24.89 | 48.53 | 0.27 | 0.71 | 5.3 | 0.19 | 2.44 |
| Ev 5.0-3 | 11.87 | 1837.8 | 157.71 | 0.57 | 5.66 | 10.36 | 20.01 | 0.34 | 0.24 | 1.7 | 0.06 | 0.69 |
| Ev 5.0-4 | 11.99 | 1835.4 | 90.05 | 0.25 | 14.45 | 28.53 | 64.41 | -0.14 | 9.51 | 5.3 | 0.19 | 2.44 |
| Ev 6.1-1 | 12.6 | 1822.9 | 81.84 | 0.2 | 8.02 | 15.54 | 30.33 | 0.04 | 0.59 | 0.6 | 0.02 | 0.2 |
| Ev 6.1-2 | 12.72 | 1820.8 | 109.47 | 0.4 | -0.79 | -0.54 | 0.53 | -0.52 | 1.54 | 3.11 | 0.11 | 1.35 |
| Ev 6.1-3 | 12.84 | 1818.1 | 172.11 | 0.62 | 4.22 | 8.05 | 15.72 | 0.08 | 0.38 | 1.43 | 0.05 | 0.57 |
| Ev 6.1-4 | 12.96 | 1816 | 129.41 | 0.49 | 7.92 | 15.12 | 29.11 | 0.16 | 0.19 | 2.26 | 0.08 | 0.95 |
| Ev 6.2-5 | 13.08 | 1813.7 | 100.46 | 0.35 | -0.63 | -0.79 | -0.14 | -0.23 | 1.35 | 3.72 | 0.13 | 1.65 |
| Ev 6.2-6 | 13.2 | 1811.9 | 266.7 | 0.75 | -10.07 | -19.55 | -38.03 | 0.05 | -1.21 | 0.9 | 0.03 | 0.34 |
| Ev 6.2-7 | 13.32 | 1809.7 | 163.59 | 0.6 | 1.36 | 2.27 | 4.05 | 0.19 | -0.27 | 1.53 | 0.05 | 0.62 |
| Ev 6.2-8 | 13.44 | 1807.8 | 65.51 | 0 | 7.75 | 14.93 | 29.28 | 0.09 | 0.71 | 0.6 | 0.02 | 0.2 |
| Ev 7.0-4 | 15.99 | 1761.7 | 112.76 | 0.29 | 11.32 | 20.63 | 42.14 | 0.75 | 2.59 | 4.6 | 0.17 | 2.08 |
| Ev 8.0-4 | 19.25 | 1696.2 | 173.27 | 0.63 | 3.29 | 5.64 | 12.02 | 0.39 | 1.28 | 1.38 | 0.05 | 0.55 |
| Ev 8.0-5 | 19.35 | 1694 | 69.74 | 0.07 | 9.24 | 17.73 | 35.01 | 0.15 | 1.06 | 0.6 | 0.02 | 0.2 |
| Ev 9.0-4 | 20.3 | 1674.2 | 136.63 | 0.48 | 6.56 | 11.57 | 22.45 | 0.62 | 0.34 | 2.35 | 0.08 | 0.99 |
| Ev 9.0-5 | 20.4 | 1672.3 | 104.02 | 0.32 | 2.42 | 3.63 | 8.5 | 0.55 | 1.6 | 4.14 | 0.15 | 1.85 |
| Ev 10.0-1 | 21.7 | 1646.4 | 62.92 | 0 | 4.15 | 8.53 | 16.76 | -0.23 | 0.49 | 0.6 | 0.02 | 0.2 |
| Ev 10.0-2 | 21.8 | 1644.2 | 196.44 | 0.68 | 2.88 | 4.89 | 7.91 | 0.36 | -1.39 | 1.15 | 0.04 | 0.45 |
| Ev 10.0-3 | 21.9 | 1642.4 | 193.02 | 0.67 | 8.57 | 14.53 | 25.14 | 1.11 | -2.65 | 1.2 | 0.04 | 0.47 |
| Ev 10.0-4 | 22 | 1640.4 | 92.6 | 0.32 | 12.48 | 23.02 | 44.16 | 0.69 | -0.04 | 4.14 | 0.15 | 1.85 |
| Ev 10.0-5 | 22.1 | 1638.3 | 77.82 | 0.19 | 8.69 | 16.83 | 32.3 | 0.06 | 0.08 | 0.6 | 0.02 | 0.2 |
| Ev 11.0-5 | 22.79 | 1623.2 | 117.8 | 0.32 | 5.1 | 9.97 | 20.41 | -0.02 | 1.38 | 4.14 | 0.15 | 1.85 |
| Ev 11.0-6 | 22.89 | 1621.1 | 85.95 | 0.07 | 8.85 | 17.18 | 33.19 | 0.04 | 0.29 | 0.6 | 0.02 | 0.2 |
| Ev 12.2-5 | 23.81 | 1599.4 | 143.2 | 0.4 | 1.15 | 1.07 | 7.7 | 0.6 | 5.66 | 3.11 | 0.11 | 1.35 |
| Ev 12.2-6 | 23.91 | 1597.3 | 122.2 | 0.29 | 14.18 | 23.21 | 41.69 | 2.29 | -2.87 | 4.6 | 0.17 | 2.08 |
| Ev 13.0-1 | 29.86 | 1466.5 | 89.57 | 0 | 6.69 | 12.91 | 25.18 | 0.07 | 0.52 | 0.6 | 0.02 | 0.2 |
| Ev 13.0-3 | 30.06 | 1462.2 | 291.09 | 0.69 | -4.3 | -7.03 | -12.08 | -0.67 | 1.24 | 1.11 | 0.04 | 0.43 |
| Ev 13.0-4 | 30.11 | 1461 | 455.12 | 0.8 | -4.01 | -6.72 | -12.07 | -0.54 | 0.66 | 0.75 | 0.03 | 0.28 |
| Ev 13.0-5 | 30.16 | 1459.7 | 459.83 | 0.81 | 0.58 | 1.04 | 1.75 | 0.04 | -0.22 | 0.73 | 0.02 | 0.27 |
| Ev 13.0-6 | 30.21 | 1458.1 | 238.57 | 0.62 | 4.94 | 8.2 | 15.3 | 0.73 | -0.34 | 1.43 | 0.05 | 0.57 |
| Ev 13.0-7 | 30.26 | 1457 | 98.58 | 0.09 | 4.01 | 7.7 | 14.91 | 0.05 | 0.22 | 0.6 | 0.02 | 0.2 |
| Ev 13.0-8 | 30.36 | 1453.6 | 97.56 | 0.08 | 7.87 | 15.18 | 29.89 | 0.08 | 0.85 | 0.6 | 0.02 | 0.2 |
| Ev 15.0-1 | 34.66 | 1352.1 | 84.85 | 0.1 | 8.55 | 16.66 | 32.5 | 0 | 0.61 | 0.6 | 0.02 | 0.2 |
| Ev 15.0-2 | 34.76 | 1350 | 84.35 | 0.09 | 7.72 | 15.17 | 29.98 | -0.06 | 0.96 | 0.6 | 0.02 | 0.2 |
| Ev 15.0-3 | 34.86 | 1347.9 | 210.71 | 0.64 | 3.93 | 6.91 | 12.03 | 0.37 | -1.15 | 1.33 | 0.05 | 0.53 |
| Ev 15.0-4 | 34.96 | 1345.8 | 171.35 | 0.55 | 9.71 | 15.99 | 28.06 | 1.51 | -2.53 | 1.83 | 0.06 | 0.75 |
| Ev 15.0-6 | 35.16 | 1341 | 76.68 | 0 | 8.44 | 16.48 | 32.28 | -0.01 | 0.74 | 0.6 | 0.02 | 0.2 |
| Ev 16.1-21 | 37.02 | 1295.2 | 98.62 | 0.19 | 5.79 | 11.63 | 23.69 | -0.18 | 1.48 | 0.6 | 0.02 | 0.2 |
| Ev 16.1-20 | 37.12 | 1292.7 | 121.99 | 0.35 | 0.77 | 1.43 | 3.35 | 0.03 | 0.63 | 3.72 | 0.13 | 1.65 |
| Ev 16.1-19 | 37.22 | 1290.3 | 199.17 | 0.6 | 1.27 | 2.91 | 4.35 | -0.22 | -1.18 | 1.53 | 0.05 | 0.62 |
| Ev 16.1-17 | 37.42 | 1285.1 | 114.25 | 0.3 | 8.74 | 15.39 | 27.78 | 0.84 | -1.66 | 4.44 | 0.16 | 2 |
| Ev 16.2-15 | 37.62 | 1280.7 | 105.46 | 0.25 | 2.98 | 7.01 | 13.27 | -0.62 | -0.09 | 5.3 | 0.19 | 2.44 |
| Ev 16.2-14 | 37.72 | 1278.5 | 256.54 | 0.69 | 1.63 | 3.39 | 7.08 | -0.12 | 0.62 | 1.11 | 0.04 | 0.43 |
| Ev 16.2-13 | 37.77 | 1277.6 | 460.59 | 0.83 | 3.2 | 5.5 | 11.04 | 0.37 | 0.57 | 0.68 | 0.02 | 0.25 |
| Ev 16.2-11 | 37.92 | 1274 | 81.97 | 0.03 | 8.17 | 15.66 | 29.84 | 0.14 | -0.12 | 0.6 | 0.02 | 0.2 |
| Ev 16.3-10 | 38.02 | 1271.8 | 147.9 | 0.46 | 4.23 | 8.39 | 16.58 | -0.08 | 0.58 | 2.52 | 0.09 | 1.07 |
| Ev 16.3-9 | 38.12 | 1269.6 | 143.52 | 0.45 | 3.67 | 6.96 | 13.73 | 0.1 | 0.47 | 2.61 | 0.09 | 1.11 |
| Ev 16.3-8 | 38.22 | 1267 | 100.83 | 0.21 | 2.58 | 5.57 | 13.39 | -0.28 | 2.79 | 6.11 | 0.22 | 2.86 |
| Ev 16.4-7 | 38.32 | 1264 | 121.1 | 0.34 | -5.42 | -8.17 | -13.41 | -1.21 | 2.07 | 3.85 | 0.14 | 1.71 |
| Ev 16.4-6 | 38.42 | 1261.4 | 499.95 | 0.84 | -5.77 | -9.71 | -17.04 | -0.76 | 1.32 | 0.65 | 0.02 | 0.24 |
| Ev 16.4-5 | 38.47 | 1260.4 | 1020.93 | 0.92 | -0.03 | 0 | 0.95 | -0.03 | 0.95 | 0.49 | 0.02 | 0.17 |
| Ev 16.4-4 | 38.52 | 1258.9 | 794.15 | 0.9 | 9.93 | 16.47 | 29.95 | 1.48 | -1.57 | 0.53 | 0.02 | 0.19 |
| Ev 16.4-3 | 38.57 | 1257.9 | 307.83 | 0.74 | 14.38 | 23.74 | 42.89 | 2.22 | -2.69 | 0.93 | 0.03 | 0.35 |
| Ev 16.4-2 | 38.62 | 1256.3 | 105.43 | 0.25 | 13.78 | 23.93 | 44.31 | 1.53 | -1.65 | 5.3 | 0.19 | 2.44 |
| Ev 16.4-1 | 38.72 | 1253.6 | 79.44 | 0 | 8.51 | 16.52 | 32.46 | 0.04 | 0.84 | 0.6 | 0.02 | 0.2 |
| Ev 17.0-6 | 39.12 | 1243.1 | 85.36 | 0.21 | 7.93 | 15.05 | 38.57 | 0.2 | 9.77 | 6.11 | 0.22 | 2.86 |
| Ev 17.0-5 | 39.24 | 1240 | 114.01 | 0.41 | 2.29 | 4.35 | 13.08 | 0.06 | 4.81 | 3.01 | 0.11 | 1.3 |
| Ev 17.0-4 | 39.36 | 1236.3 | 120.82 | 0.44 | -0.01 | 1.76 | 8.72 | -0.92 | 5.37 | 2.7 | 0.1 | 1.16 |
| Ev 17.0-3 | 39.48 | 1233.1 | 231.61 | 0.71 | -1.71 | -2.36 | -1.98 | -0.49 | 2.49 | 1.04 | 0.04 | 0.4 |
| Ev 17.0-2 | 39.6 | 1230 | 131.59 | 0.49 | 10.69 | 18.15 | 35.38 | 1.38 | 0.61 | 2.26 | 0.08 | 0.95 |
| Ev 17.0-1 | 39.72 | 1227.1 | 67.44 | 0 | 7.81 | 15.17 | 24.33 | 0.03 | -4.68 | 0.6 | 0.02 | 0.2 |
| Ev 18.1-12 | 41.17 | 1191 | 139.53 | 0.55 | 6.78 | 12.79 | 30.73 | 0.22 | 6.3 | 1.83 | 0.06 | 0.75 |
| Ev 18.1-11 | 41.24 | 1188.9 | 101.31 | 0.37 | 8.54 | 16.59 | 39.35 | 0.03 | 7.59 | 3.46 | 0.12 | 1.52 |
| Ev 18.2-5 | 41.85 | 1172.3 | 378.46 | 0.83 | 3.28 | 6.31 | 14.4 | 0.04 | 2.39 | 0.68 | 0.02 | 0.25 |
| Ev 18.2-4 | 41.9 | 1170.8 | 282.73 | 0.78 | 8.19 | 14.44 | 26.79 | 0.78 | -0.83 | 0.81 | 0.03 | 0.3 |
| Ev 18.2-3 | 41.95 | 1169.4 | 161.54 | 0.61 | 6.86 | 12.77 | 25 | 0.3 | 0.59 | 1.48 | 0.05 | 0.59 |
| Ev 19.0-5 | 44.42 | 1110.2 | 144.17 | 0.47 | 2.16 | 4.59 | 9.33 | -0.2 | 0.6 | 2.43 | 0.09 | 1.03 |
| Ev 21.1-3 | 47.2 | 1039.5 | 101.4 | 0.1 | 8.43 | 15.73 | 30.03 | 0.36 | -0.06 | 0.6 | 0.02 | 0.2 |
| Ev 21.2-6 | 47.5 | 1031.1 | 125.29 | 0.27 | 12.69 | 23.3 | 42.49 | 0.76 | -2.25 | 4.94 | 0.18 | 2.26 |
| Ev 22.0-1 | 50.04 | 965.6 | 89.93 | 0 | 7.56 | 14.61 | 29.16 | 0.06 | 1.22 | 0.6 | 0.02 | 0.2 |
| Ev 22.0-2 | 50.12 | 963.7 | 142.87 | 0.37 | 5.75 | 10.61 | 18.92 | 0.3 | -1.34 | 3.46 | 0.12 | 1.52 |
| Ev 22.0-3 | 50.2 | 961.7 | 197.73 | 0.55 | 6.63 | 11.75 | 20.81 | 0.6 | -1.62 | 1.83 | 0.06 | 0.75 |
| Ev 22.0-4 | 50.28 | 959.8 | 158.93 | 0.43 | 4.09 | 7.16 | 11.85 | 0.41 | -1.79 | 2.8 | 0.1 | 1.2 |
| Ev 22.0-5 | 50.36 | 957.3 | 91.41 | 0.02 | 7.56 | 14.44 | 28.35 | 0.15 | 0.73 | 0.6 | 0.02 | 0.2 |
| Ev 23.0-4 | 52.53 | 901.1 | 159 | 0.48 | 11.4 | 19.34 | 35.24 | 1.48 | -1.83 | 2.35 | 0.08 | 0.99 |
| Ev 24.2-4 | 54.16 | 856.9 | 99.64 | 0.14 | 2.06 | 3.53 | 6.62 | 0.25 | -0.1 | 0.6 | 0.02 | 0.2 |
| Ev 25.0-5 | 55.65 | 818.7 | 125.95 | 0.32 | 9.01 | 16.47 | 32.91 | 0.56 | 1.38 | 4.14 | 0.15 | 1.85 |
| Ev 27.2-10 | 60.78 | 682.5 | 133.57 | 0.38 | 0.2 | 0.86 | 1.79 | -0.24 | 0.14 | 3.34 | 0.12 | 1.46 |
| Ev 28.0-4 | 63.25 | 610.1 | 133.72 | 0.44 | 9.34 | 16.95 | 31.11 | 0.65 | -1.34 | 2.7 | 0.1 | 1.16 |
| Ev 30.0-1 | 64.3 | 581.1 | 99.4 | 0 | 7.3 | 14.11 | 27.5 | 0.06 | 0.52 | 0.6 | 0.02 | 0.2 |
| Ev 30.0-2 | 64.38 | 579.1 | 150.2 | 0.33 | -1.93 | -2.83 | -4.52 | -0.47 | 0.85 | 3.99 | 0.14 | 1.78 |
| Ev 30.0-3 | 64.46 | 577.1 | 324 | 0.69 | 0.69 | 1 | 1.62 | 0.18 | -0.28 | 1.11 | 0.04 | 0.43 |
| Ev 30.0-4 | 64.5 | 576.1 | 318.5 | 0.68 | 3.83 | 6.05 | 10.06 | 0.71 | -1.47 | 1.15 | 0.04 | 0.45 |
| Ev 30.0-5 | 64.54 | 575 | 206.7 | 0.51 | 4.22 | 6.93 | 13.04 | 0.66 | -0.17 | 2.11 | 0.07 | 0.88 |
| Ev 30.0-6 | 64.62 | 572.8 | 109.2 | 0.07 | 10.63 | 20.37 | 39.94 | 0.19 | 0.88 | 0.6 | 0.02 | 0.2 |
| Ev 31.0-1 | 65.52 | 547.7 | 103 | 0 | 7.5 | 14.42 | 28.18 | 0.1 | 0.61 | 0.6 | 0.02 | 0.2 |
| Ev 31.0-2 | 65.6 | 545.1 | 159 | 0.35 | -2.19 | -3.71 | -6.41 | -0.28 | 0.63 | 3.72 | 0.13 | 1.65 |
| Ev 31.0-3 | 65.68 | 543 | 264 | 0.61 | -0.39 | -0.88 | -1.95 | 0.07 | -0.27 | 1.48 | 0.05 | 0.59 |
| Ev 31.0-4 | 65.76 | 541 | 163.5 | 0.37 | 4.84 | 7.53 | 12.24 | 0.97 | -2.12 | 3.46 | 0.12 | 1.52 |
| Ev 31.0-5 | 65.84 | 538.4 | 125 | 0.18 | 5.98 | 11.38 | 21.77 | 0.13 | 0.03 | 0.6 | 0.02 | 0.2 |
| Ev 31.0-6 | 65.92 | 536.4 | 103 | 0 | 8.19 | 15.89 | 30.78 | 0.04 | 0.38 | 0.6 | 0.02 | 0.2 |
| Ev 32.0-4 | 67.6 | 490.6 | 128.6 | 0.37 | 2.87 | 5.4 | 10.05 | 0.09 | -0.24 | 3.46 | 0.12 | 1.52 |

| | | | | | | | | | | | | |
|---|---|---|---|---|---|---|---|---|---|---|---|---|
| Ev30.0-4 | 64.5 | 576.1 | 318.5 | 0.68 | 3.83 | 6.05 | 10.06 | 0.71 | -1.47 | 1.15 | 0.04 | 0.45 |
| Ev30.0-5 | 64.54 | 575 | 206.7 | 0.51 | 4.22 | 6.93 | 13.04 | 0.66 | -0.17 | 2.11 | 0.07 | 0.88 |
| Ev30.0-6 | 64.62 | 572.8 | 109.2 | 0.07 | 10.63 | 20.37 | 39.94 | 0.19 | 0.88 | 0.6 | 0.02 | 0.2 |
| Ev31.0-1 | 65.52 | 547.7 | 103 | 0 | 7.5 | 14.42 | 28.18 | 0.1 | 0.61 | 0.6 | 0.02 | 0.2 |
| Ev31.0-2 | 65.6 | 545.1 | 159 | 0.35 | -2.19 | -3.71 | -6.41 | -0.28 | 0.63 | 3.72 | 0.13 | 1.65 |
| Ev31.0-3 | 65.68 | 543 | 264 | 0.61 | -0.39 | -0.88 | -1.95 | 0.07 | -0.27 | 1.48 | 0.05 | 0.59 |
| Ev31.0-4 | 65.76 | 541 | 163.5 | 0.37 | 4.84 | 7.53 | 12.24 | 0.97 | -2.12 | 3.46 | 0.12 | 1.52 |
| Ev31.0-5 | 65.84 | 538.4 | 125 | 0.18 | 5.98 | 11.38 | 21.77 | 0.13 | 0.03 | 0.6 | 0.02 | 0.2 |
| Ev31.0-6 | 65.92 | 536.4 | 103 | 0 | 8.19 | 15.89 | 30.78 | 0.04 | 0.38 | 0.6 | 0.02 | 0.2 |
| Ev32.0-4 | 67.6 | 490.6 | 128.6 | 0.37 | 2.87 | 5.4 | 10.05 | 0.09 | -0.24 | 3.46 | 0.12 | 1.52 |
| Ev33.0-4 | 69.46 | 434.2 | 145 | 0.39 | 5.17 | 9 | 17.64 | 0.54 | 0.48 | 3.23 | 0.12 | 1.41 |
| Ev33.0-5 | 69.52 | 432.6 | 88 | 0 | 8.54 | 16.48 | 31.71 | 0.08 | 0.16 | 0.6 | 0.02 | 0.2 |
| Ev35.0-2 | 75.95 | 240.4 | 176.6 | 0.54 | 1.71 | 3.54 | 6.99 | -0.11 | 0.26 | 1.9 | 0.07 | 0.78 |
| Ev35.0-3 | 76.04 | 237.6 | 186.31 | 0.56 | 0.55 | 0.92 | 1.99 | 0.07 | 0.24 | 1.77 | 0.06 | 0.72 |
| Ev35.0-4 | 76.13 | 235 | 112.65 | 0.28 | 8.41 | 15.33 | 27.75 | 0.54 | -1.58 | 4.77 | 0.17 | 2.17 |
| Ev37.0-1 | 77.05 | 209.7 | 140 | 0.31 | -1.59 | -2.47 | -5.17 | -0.31 | -0.49 | 4.29 | 0.16 | 1.93 |
| Ev37.0-2 | 77.13 | 207.6 | 164.3 | 0.41 | -9.18 | -18.05 | -36.03 | 0.15 | -2.01 | 3.01 | 0.11 | 1.3 |
| Ev37.0-3 | 77.21 | 205 | 129.4 | 0.25 | 6.06 | 11.71 | 20.08 | 0.05 | -2.29 | 5.3 | 0.19 | 2.44 |
| Ev37.0-4 | 77.29 | 202.4 | 97.02 | 0 | 7.06 | 13.63 | 26.8 | 0.07 | 0.75 | 0.6 | 0.02 | 0.2 |
| Ev38.0-1 | 78.18 | 176 | 103.33 | 0 | 6.73 | 13.2 | 26.05 | -0.05 | 0.83 | 0.6 | 0.02 | 0.2 |
| Ev38.0-2 | 78.26 | 173.3 | 158.08 | 0.35 | -4.68 | -8.49 | -16.77 | -0.3 | -0.7 | 3.72 | 0.13 | 1.65 |
| Ev38.0-4 | 78.42 | 168.5 | 121.4 | 0.15 | 6.57 | 12.59 | 24.33 | 0.1 | 0.28 | 0.6 | 0.02 | 0.2 |
| Ev38.0-5 | 78.5 | 166.5 | 113 | 0.09 | 7.57 | 14.62 | 28.58 | 0.07 | 0.61 | 0.6 | 0.02 | 0.2 |
| Ev40.0-3 | 84.55 | -5.5 | 176.44 | 0.41 | 7.95 | 14.68 | 26.31 | 0.42 | -1.76 | 3.01 | 0.11 | 1.3 |
| Ev40.0-4 | 84.6 | -6.8 | 176.3 | 0.41 | 8.93 | 16.51 | 30.02 | 0.46 | -1.58 | 3.01 | 0.11 | 1.3 |
| Ev41.0-3 | 85.42 | -35.9 | 122.36 | 0.28 | -1.95 | -3.96 | -7.82 | 0.09 | -0.31 | 4.77 | 0.17 | 2.17 |
| Ev41.0-4 | 85.49 | -38.3 | 126.27 | 0.3 | 4.9 | 9.4 | 18.3 | 0.06 | 0.36 | 4.44 | 0.16 | 2 |
| Ev44.0-1 | 87.56 | -118.6 | 81.39 | 0 | 4.46 | 8.58 | 16.39 | 0.06 | 0.03 | 0.6 | 0.02 | 0.2 |
| Ev44.0-2 | 87.64 | -120.7 | 137.61 | 0.41 | 9.26 | 14.26 | 27.41 | 1.94 | 0.14 | 3.01 | 0.11 | 1.3 |
| Ev44.0-3 | 87.72 | -123.6 | 180.24 | 0.55 | 5.43 | 10.31 | 18.86 | 0.14 | -0.82 | 1.83 | 0.06 | 0.75 |
| Ev44.0-4 | 87.8 | -125.7 | 184.93 | 0.56 | 9.17 | 16.77 | 30.63 | 0.56 | -1.48 | 1.77 | 0.06 | 0.72 |
| Ev44.0-5 | 87.88 | -128.5 | 106.22 | 0.23 | 14.68 | 28.57 | 55.53 | 0.07 | 0.54 | 5.69 | 0.21 | 2.64 |
| Ev46.1-1 | 90.22 | -204.6 | 94.79 | 0.33 | 6.6 | 13.28 | 27.1 | -0.21 | 1.72 | 3.99 | 0.14 | 1.78 |
| Ev46.1-2 | 90.31 | -207.3 | 181.27 | 0.65 | 2.83 | 5.65 | 11.01 | -0.08 | 0.24 | 1.28 | 0.04 | 0.51 |
| Ev46.1-3 | 90.4 | -210.1 | 253.38 | 0.75 | 4.53 | 8.21 | 15.16 | 0.32 | -0.49 | 0.9 | 0.03 | 0.34 |
| Ev46.1-4 | 90.45 | -212 | 224.09 | 0.72 | 5.7 | 10.02 | 18.14 | 0.56 | -0.98 | 1 | 0.03 | 0.38 |
| Ev46.1-5 | 90.49 | -213.2 | 151.6 | 0.58 | 6.71 | 12.42 | 22.56 | 0.33 | -1.18 | 1.65 | 0.06 | 0.67 |
| Ev46.1-6 | 90.58 | -215.4 | 120.01 | 0.47 | 5.57 | 10.91 | 21.23 | -0.04 | 0.4 | 2.43 | 0.09 | 1.03 |
| Ev46.1-7 | 90.67 | -217.7 | 101.27 | 0.37 | 6.28 | 11.46 | 20.81 | 0.4 | -1.07 | 3.46 | 0.12 | 1.52 |
| Ev46.2-8 | 90.76 | -220.8 | 84.31 | 0.25 | 9.68 | 17.94 | 33.37 | 0.48 | -0.99 | 5.3 | 0.19 | 2.44 |
| Ev46.2-9 | 90.85 | -223.7 | 105.46 | 0.4 | 7.15 | 14.1 | 27.79 | -0.09 | 0.83 | 3.11 | 0.11 | 1.35 |
| Ev46.2-10 | 90.94 | -226.6 | 126.76 | 0.5 | 5.26 | 10 | 19.01 | 0.12 | -0.08 | 2.18 | 0.08 | 0.91 |
| Ev46.2-11 | 91.03 | -230.2 | 126.7 | 0.5 | 6.26 | 12.16 | 23.69 | 0.02 | 0.46 | 2.18 | 0.08 | 0.91 |
| Ev46.2-12 | 91.12 | -233.3 | 125.93 | 0.5 | 6.02 | 11.8 | 23.17 | -0.04 | 0.63 | 2.18 | 0.08 | 0.91 |
| Ev46.2-13 | 91.21 | -236.1 | 72.64 | 0.13 | 8.24 | 15.92 | 30.89 | 0.07 | 0.42 | 0.6 | 0.02 | 0.2 |
| Ev46.3-15 | 91.39 | -241.3 | 76.87 | 0.18 | 8.97 | 17.45 | 33.48 | 0.02 | 0.06 | 0.6 | 0.02 | 0.2 |
| Ev46.3-16 | 91.48 | -243.9 | 118.02 | 0.46 | 3.01 | 6.9 | 14.19 | -0.53 | 1.04 | 2.52 | 0.09 | 1.07 |
| Ev46.3-17 | 91.57 | -247.2 | 166.45 | 0.62 | 6.86 | 12.85 | 25.22 | 0.27 | 0.67 | 1.43 | 0.05 | 0.57 |
| Ev46.3-18 | 91.66 | -249.9 | 126.85 | 0.5 | 4.72 | 8.48 | 15.81 | 0.36 | -0.36 | 2.18 | 0.08 | 0.91 |
| Ev46.3-19 | 91.75 | -252.6 | 96.46 | 0.34 | -8.5 | -17.04 | -33.25 | 0.31 | -1.13 | 3.85 | 0.14 | 1.71 |
| Ev48.0-1 | 94.71 | -343.3 | 146.71 | 0.34 | -0.96 | -1.8 | -3.55 | -0.04 | -0.13 | 3.85 | 0.14 | 1.71 |
| Ev48.0-2 | 94.79 | -345.5 | 155.73 | 0.38 | 0.18 | 0.31 | 0.66 | 0.01 | 0.06 | 3.34 | 0.12 | 1.46 |
| Ev48.0-3 | 94.87 | -348.1 | 97.23 | 0 | 7.86 | 15.26 | 29.63 | 0.03 | 0.45 | 0.6 | 0.02 | 0.2 |
| Ev49.0-1 | 97.06 | -422.7 | 128.22 | 0.3 | -6.25 | -10.27 | -16.27 | -0.94 | 3.15 | 4.44 | 0.16 | 2 |
| Ev49.0-2 | 97.15 | -426.4 | 323.36 | 0.72 | -3.71 | -6 | -9.6 | -0.61 | 1.78 | 1 | 0.03 | 0.38 |
| Ev49.0-3 | 97.2 | -427.9 | 350.67 | 0.74 | 6.82 | 11.39 | 20.91 | 0.97 | -0.84 | 0.93 | 0.03 | 0.35 |
| Ev49.0-4 | 97.24 | -429.3 | 194.83 | 0.54 | 7.91 | 13.89 | 24.97 | 0.78 | -1.59 | 1.9 | 0.07 | 0.78 |
| Ev49.0-5 | 97.33 | -432.1 | 144.7 | 0.38 | 9.29 | 17.19 | 30.95 | 0.48 | -1.97 | 3.34 | 0.12 | 1.46 |
| Ev49.0-6 | 97.42 | -435.5 | 115.1 | 0.22 | 3.68 | 7.11 | 14.39 | 0.03 | 0.84 | 5.9 | 0.22 | 2.75 |
| Ev49.0-7 | 97.51 | -438.2 | 90.21 | 0 | 8.32 | 15.93 | 30.53 | 0.14 | 0.04 | 0.6 | 0.02 | 0.2 |
| Ev50.1-1 | 98.16 | -460.3 | 103.19 | 0.25 | 8.81 | 17.37 | 33.2 | -0.1 | -0.06 | 5.3 | 0.19 | 2.44 |
| Ev50.1-2 | 98.25 | -463.1 | 137.38 | 0.43 | 8.13 | 15.97 | 30.85 | -0.06 | 0.28 | 2.8 | 0.1 | 1.2 |
| Ev50.1-3 | 98.34 | -466.6 | 162.93 | 0.52 | 6.52 | 12.79 | 24.34 | -0.05 | -0.1 | 2.04 | 0.07 | 0.84 |
| Ev50.2-5 | 98.52 | -472.2 | 129.28 | 0.4 | 3.64 | 7.31 | 14.31 | -0.12 | 0.38 | 3.11 | 0.11 | 1.35 |
| Ev50.2-6 | 98.61 | -475.7 | 104.23 | 0.25 | 1.05 | 2.37 | 4.48 | -0.17 | -0.03 | 5.3 | 0.19 | 2.44 |
| Ev50.3-7 | 98.7 | -478.3 | 93.35 | 0.17 | 8.51 | 16.43 | 31.58 | 0.09 | 0.14 | 0.6 | 0.02 | 0.2 |
| Ev50.3-8 | 98.79 | -480.9 | 130.19 | 0.4 | 3.69 | 7.19 | 13.69 | 0 | -0.01 | 3.11 | 0.11 | 1.35 |
| Ev50.3-9 | 98.88 | -483.6 | 136.64 | 0.43 | 1.92 | 3.53 | 6.31 | 0.11 | -0.41 | 2.8 | 0.1 | 1.2 |
| Ev50.3-10 | 98.97 | -487 | 77.83 | 0 | 8.84 | 17.07 | 32.94 | 0.09 | 0.26 | 0.6 | 0.02 | 0.2 |
| Ev51.0-1 | 99.88 | -518.2 | 86.02 | 0 | 9.06 | 17.67 | 34.14 | 0 | 0.3 | 0.6 | 0.02 | 0.2 |
| Ev51.0-2 | 99.97 | -521.9 | 109.34 | 0.21 | 2.9 | 5.99 | 11.3 | -0.18 | -0.11 | 6.11 | 0.22 | 2.86 |
| Ev51.0-3 | 100.06 | -524.8 | 147.62 | 0.42 | -1.12 | -1.75 | -2.98 | -0.22 | 0.34 | 2.9 | 0.1 | 1.25 |
| Ev51.0-4 | 100.15 | -528.5 | 173.35 | 0.5 | 0.75 | 1.13 | 1.94 | 0.17 | -0.21 | 2.18 | 0.08 | 0.91 |
| Ev51.0-5 | 100.24 | -530.8 | 98.46 | 0.13 | 2.98 | 5.59 | 10.92 | 0.11 | 0.27 | 0.6 | 0.02 | 0.2 |

**Dataset S1.** Isotopic results used in that study, with associated uncertainties. Isotopic values are background-corrected for volcanic fractions > 0.2. Otherwise, mass-spectrometer values are given and uncertainties do not take into account error propagation. Top depth represents the depth in core 1 of the top of the sample, and "estimated age" corresponds to the age of this depth.


Au Yang, D., Landais, G., Assayag, N., Widory, D., & Cartigny, P. (2016). Improved analysis of micro- and nanomole-scale sulfur multi-isotope compositions by gas source isotope ratio mass spectrometry. *Rapid Communications in Mass Spectrometry, 30*(7), 897-907. doi:10.1002/rcm.7513

Bekki, S. (1995). Oxidation of volcanic SO2: a sink for stratospheric OH and H2O. *Geophysical Research Letters, 22*(8), 913-916.

Cadoux, A., Scaillet, B., Bekki, S., Oppenheimer, C., & Druitt, T. H. (2015). Stratospheric Ozone destruction by the Bronze-Age Minoan eruption (Santorini Volcano, Greece). *Scientific reports, 5*, 12243.

Castleman, A. W. J., Munkelwitz, H. R., & Manowitz, B. (1974). Isotopic studies of the sulfur component of the stratospheric aerosol layer. *Tellus, 26*, 222-234.

Endo, Y., Ueno, Y., Aoyama, S., & Danielache, S. O. (2016). Sulfur isotope fractionation by broadband UV radiation to optically thin SO2 under reducing atmosphere. *Earth and Planetary Science Letters, 453*, 9-22. doi:10.1016/j.epsl.2016.07.057

Gautier, E. (2015). *Empreinte isotopique et histoire du volcanisme stratosphérique des 2600 dernières années, enregistrées à Dôme C, Antarctique.* (PhD Dissertation), Université Grenoble-Alpes, Grenoble.

Gautier, E., Savarino, J., Erbland, J., Lanciki, A., & Possenti, P. (2016). Variability of sulfate signal in ice core records based on five replicate cores. *Climate of the Past, 12*(1), 103-113. doi:10.5194/cp-12-103-2016

Harris, E., Sinha, B., Hoppe, P., Crowley, J. N., Ono, S., & Foley, S. (2012). Sulfur isotope fractionation during oxidation of sulfur dioxide: gas-phase oxidation by OH radicals and aqueous oxidation by H2O2, O3 and iron catalysis. *Atmospheric Chemistry and Physics, 12*(1), 407-423. doi:10.5194/acp-12-407-2012

Hattori, S., Schmidt, J. A., Johnson, M. S., Danielache, S. O., Yamada, A., Ueno, Y., & Yoshida, N. (2013). SO2 photoexcitation mechanism links mass-independent sulfur isotopic fractionation in cryospheric sulfate to climate impacting volcanism. *Proceedings of the National Academy of Sciences of the United States of America, 110*(44), 17656-17661. doi:10.1073/pnas.1213153110

Junge, E., Manson, J. E., & Studies, J. (1961). Stratospheric aerosol studies. *Journal of Geophysical Research, 66*(7), 2156-2202. doi:10.1029/JZ066i007p02163

Oduro, H., Harms, B., Sintim, H. O., Kaufman, A. J., Cody, G., & Farquhar, J. (2011). Evidence of magnetic isotope effects during thermochemical sulfate reduction. *Proceedings of the National Academy of Sciences of the United States of America, 108*(43), 17635-17638. doi:10.1073/pnas.1108112108

Patris, N., Mihalopoulos, N., Baboukas, E. D., & Jouzel, J. (2000). Isotopic composition of sulfur in size-resolved marine aerosols above the Atlantic Ocean. *Journal of Geophysical Research, 105*(D11), 14449-14457.

Rees, C. E., Jenkins, W. J., & Monster, J. (1978). The sulphur isotopic composition of ocean water sulphate, . *Geochimica Et Cosmochimica Acta, 42*(65), 377-381.

Seinfeld, J. H., & Pandis, S. N. (1998). *Atmospheric chemistry and physics*. New York, USA: John Wiley & Sons.

Taylor, J. R. (1997). An Introduction to Error Analysis: The study of un-certainties in physical measurements. *University Science Books, 2 Edn.*

Thode, H. G., Monster, J., & Dunford, H. B. (1961). Sulphur isotope geochemistry. *Geochimica Et Cosmochimica Acta, 25*(3), 159-174.

von Glasow, R. (2010). Atmospheric chemistry in volcanic plumes. *Proceedings of the National Academy of Sciences of the United States of America, 107*(15), 6594-6599. doi:10.1073/pnas.0913164107

Whitehill, A. R., Jiang, B., Guo, H., & Ono, S. (2015). $SO_2$ photolysis as a source for sulfur mass-independent isotope signatures in stratospehric aerosols. *Atmospheric Chemistry and Physics, 15*(4), 1843-1864. doi:10.5194/acp-15-1843-2015

Whitehill, A. R., & Ono, S. (2012). Excitation band dependence of sulfur isotope mass-independent fractionation during photochemistry of sulfur dioxide using broadband light sources. *Geochimica Et Cosmochimica Acta, 94*, 238-253. doi:10.1016/j.gca.2012.06.014